Comparison of Peak-To-Peak Current Ripple Amplitude in Multiphase PWM Voltage Source Inverters

Gabriele Grandi, Jelena Loncarski, Claudio Rossi
Dept. of Electrical Engineering, University of Bologna, Italy
Viale Risorgimento 2, 40136 Bologna, Italy
Tel: +39-0512093571, Fax: +39-0512093588.
E-mail: gabriele.grandi@unibo.it, jelena.loncarski2@unibo.it, claudio.rossi@unibo.it
URL: http://www.dei.unibo.it/en

Keywords

DC-AC power conversion, Inverters, Current distribution, Distortion, Pulse width modulation.

Abstract

Multiphase systems are nowadays considered for various industrial applications. Numerous PWM schemes for multiphase voltage source inverters with sinusoidal outputs have been developed, but just recently the impact of these modulation schemes on the output peak-to-peak current ripple amplitude has been considered. Determination of current ripple in multiphase PWM voltage source inverters is important for both design and control purposes. This paper gives the comparison of the peak-to-peak current ripple distribution over a fundamental period for multiphase VSIs, starting from three-phase and extended to the multiphase inverters, with emphasis on five and seven phases. Simplified expressions to get maximum value of the ripple are carried out and compared among inverters with different phase number. Although reference is made to the centered symmetrical PWM, being the most simple and effective solution to maximize the dc bus utilization, leading to a nearly-optimal modulation to minimize the rms of the current ripple, the analysis can be readily extended to either discontinuous or asymmetrical modulations, both carrier-based and space vector PWM. The results obtained by the proposed analytical approach are backed with the numerical simulations of the peak-to-peak ripple for inverters with different phase numbers and in case of different modulation indexes to prove the effectiveness of mathematical developments.

Introduction

Multiphase power systems have many advantages over the traditional 3-phase counterparts. As an example, multiphase motor drives have the ability to reduce the amplitude and increase the frequency of torque pulsations, to reduce the rotor harmonic current losses and to lower the dc link current harmonics. Additionally, multiphase systems improve the reliability owing to their redundant structure [1]-[4]. The increase of the number of phases is a viable solution to overcome the problems related to high-power applications. In the past decades, multilevel 3-phase inverters have emerged as a promising solution in achieving high power ratings with voltage limited devices. Similarly, the use of multiphase inverters together with multiphase ac machines has been recognized as a viable approach to obtain high power ratings with current limited devices.

The behavior of multiphase systems can be represented by the multiple space vector theory, as a natural extension of the traditional 3-phase space vector transformation, leading to an elegant and effective vectorial approach in multiple α–β planes [5]. In particular, the space vectors can be usefully adopted for the modulation of multiphase inverters. The space vector modulation (SVM) for 5-phase voltage source inverters (VSIs) has been developed in [6]-[9]. Analysis of 7-phase inverters and their modulation is given in [10]-[12]. In general, for any number of phases, it has been proven that the space-vector (SV) PWM provides the same switching pattern such as the carried-based (CB) PWM in case of proper common-mode voltage injection into the modulating signals. In particular, centering the modulation signals corresponds to equally share the vector between the two null configurations [12].

Recent studies about rms output current ripple in multiphase motor drives are presented in [13]-[17], considering a 5-phase system. In [13] the optimal value of the common-mode voltage injection in CB-PWM has been analytically determined to minimize the rms current ripple in each switching period. Furthermore, it is shown that the strategy called SV-PWM, corresponding to centered and symmetric modulation, has a nearly-optimal behavior in term of the current ripple rms. In [14] it is shown that output current ripple rms cannot be minimized by injection of fifth harmonic and its odd multiples, but it is also pointed out that, from the practical point of view, differences in current ripple rms are relatively small considering sinusoidal PWM and SV-PWM. Further analysis of rms current ripple have been presented in [15]-[17]. The importance of the peak-to-peak current ripple evaluation, in addition to the rms analysis, was recently recognized in [18], where the ripple amplitude is investigated for 3-phase PWM inverters. A similar investigation is presented in [19], with detailed analytical expressions of a peak-to-peak current ripple distribution over a fundamental period. Simple and effective expressions to determine the maximum and the minimum of the current ripple amplitude in the fundamental period are also given. The analysis of the peak-to-peak current ripple amplitude was extended to multiphase systems in [20] for 5-phase VSIs and in [21] for 7-phase VSIs.

In both 3-phase and multiphase inverters, the knowledge of the peak-to-peak current ripple distribution can be useful to determine the output voltage distortion due to the inverter dead-time in case of output currents with high ripple, by determining the multiple zero-crossing interval, as proposed in [22] for the 3-phase systems. The effects of high-ripple currents on dead-time with adaptive compensation are studied in [23] and [24] as well, where the knowledge of peak-to-peak current ripple was of interest, but it has not been properly addressed. Another example of application is referred to hysteresis current controllers and variable switching frequency PWM, for single-phase [25] and three-phase inverters [26]-[28]. Furthermore, the peak-to-peak current ripple amplitude, in addition to the fundamental current component, is useful to determine the absolute current peak, affecting the thresholds of protection systems and the design of power components.

This paper gives the comparison of the analysis of peak-to-peak output current ripple already developed by the authors in [19] for 3-phase inverters, in [20] for 5-phase inverters, and in [21] for 7-phase inverters. Reference is made to centered and symmetrical switching patterns, generated either by CB- or SV-PWM. Maximum of the peak-to-peak current ripple, already been developed with given simplified and effective expressions, is here compared among cases with different number of phases. The instantaneous current ripple is introduced for a generic balanced multiphase loads consisting of series RL impedance and ac back emf (RLE). The analysis could be extended to multiphase ac motor drives as well, but the analytical model of the specific ac motor must be carefully considered to evaluate the cases in which it can be reduced to the basic RLE circuit [14], [17]. In order to compare the cases with different phase number, the analytical developments are verified by numerical simulations with a realistic inverter-RL load circuit model, represented in Fig. 1, implemented by the Simulink tool of Matlab.

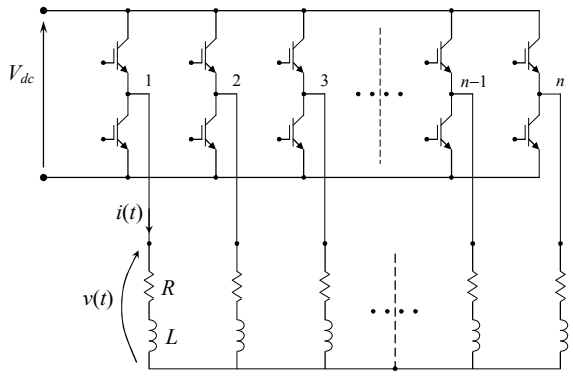

Fig. 1: Multiphase VSI supplying a RL load.

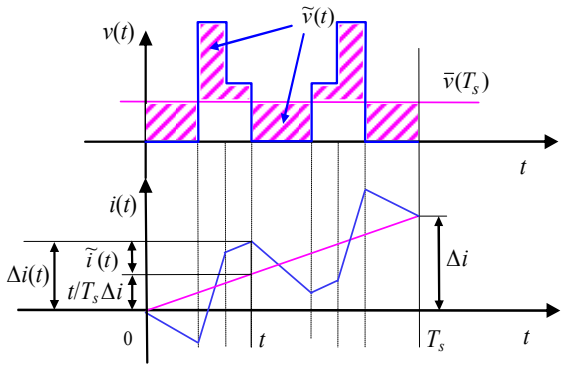

Fig. 2: Details of generic PWM output voltage and current ripple in the switching period.

Review of peak-to-peak current ripple evaluation in multiphase inverters

Definition of current ripple

Basic circuit scheme for a multiphase inverter supplying a balanced RL load is presented in Fig. 1. The voltage equation for each phase in the more general case of ac back emf (RLE) can be written as

$$v(t) = R\,i(t) + L\frac{di}{dt} + v_g(t)\,. \tag{1}$$

By averaging (1) over the switching period T_s leads to

$$\bar{v}(T_s) = R\,\bar{i}(T_s) + L\,\frac{\Delta i}{T_s} + \bar{v}_g(T_s)\,, \tag{2}$$

being $\Delta i = i(T_s) - i(0)$. (3)

The alternating component of inverter voltage can be written by introducing the average over the switching period as

$$\tilde{v}(t) = v(t) - \bar{v}(T_s)\,. \tag{4}$$

By introducing (1) and (2) in (4) leads to

$$\tilde{v}(t) = R\left[i(t) - \bar{i}(T_s)\right] + L\left[\frac{di}{dt} - \frac{\Delta i}{T_s}\right] + \left[v_g(t) - \bar{v}_g(T_s)\right]. \tag{5}$$

The expression of alternating voltage component can be simplified since the first and the third (last) term in (5) are negligible with respect to the second term, leading to

$$\tilde{v}(t) \cong L\left[\frac{di}{dt} - \frac{\Delta i}{T_s}\right]. \tag{6}$$

The current variation in the sub-period [0 – t], also depicted in Fig. 2, can be calculated from (6) as

$$\Delta i(t) \cong \frac{1}{L}\int_0^t \tilde{v}(t)dt + \frac{t}{T_s}\Delta i\,. \tag{7}$$

Eq. (7) allows defining the instantaneous current ripple as

$$\tilde{i}\,(t) = \Delta i(t) - \frac{t}{T_s}\Delta i \cong \frac{1}{L}\int_0^t \tilde{v}(t)dt\,. \tag{8}$$

Finally, the peak-to-peak current ripple amplitude can be calculated as

$$\tilde{i}_{pp} = max\left\{\tilde{i}\,(t)\right\}_0^{T_s} - min\left\{\tilde{i}\,(t)\right\}_0^{T_s}. \tag{9}$$

Multiple space vectors and pulse width modulation

For the n-phase system $\{x_1, x_2, x_3, \ldots x_n\}$, the ($n$-1)/2 space vectors, used to represent voltage and current phase quantities, lie in the planes α_1–β_1, α_3–β_3,..., α_{n-2}–β_{n-2}, respectively, and are expressed as

$$x_0 = \frac{1}{n}\sum_{k=1}^{n} x_k\,, \tag{10}$$

$$\boldsymbol{x}_h = \frac{2}{n}\sum_{k=1}^{n} x_k\,\alpha^{h(k-1)}\,,\ h = 1, 3, \ldots, n-2 \tag{11}$$

being $\alpha = exp\ (j2\pi/n)$. In (10) x_0 is the zero-sequence (homopolar) component, equal to zero in balanced systems, and in (11) $\boldsymbol{x}_h$ is the h-th component of multiple space vectors [5].

The inverse multiple space vector transformations are [5]:

$$x_k = x_0 + \sum_{h=1}^{n} \boldsymbol{x}_h \cdot \alpha^{h(k-1)}, \quad k = 1, 2, \ldots, n, \quad h = 1, 3, \ldots, n-2. \tag{12}$$

The SV-PWM of multiphase inverters is based on the determination of application times of active and null inverter voltage vectors $\boldsymbol{v}_1$, $\boldsymbol{v}_3$,…, $\boldsymbol{v}_{n-2}$ in every switching period T_s. In the case of symmetrical SV-PWM, the sequence is determined in T_s /2 and it is repeated symmetrically in the next half of the switching period. By equally sharing the application time of the zero voltage vector between the null switch configurations, the so-called "centered" switching pattern is realized and a nearly-optimal modulation able to minimize the rms of current ripple is obtained, as in the case of 3-phase [29] and 5-phase inverters [13]. This SV-PWM provides the same switching pattern such as the CB-PWM when a "min/max centering" common-mode voltage is injected into the modulating signals [30]. As result of the SV-PWM, for each phase, the average of the inverter output voltage $\bar{v}(T_s)$ corresponds to the reference voltage v^*.

In the case of sinusoidal balanced output voltages supplying a balanced load, the zero-sequence component is null. In this case, introducing the modulation index $m = V^*/V_{dc}$, the reference space voltage vectors become

$$\begin{cases} \boldsymbol{v}_1^* = \boldsymbol{v}^* = mV_{dc}e^{j\vartheta} \\ \boldsymbol{v}_3^* = 0 \\ \ldots \\ \boldsymbol{v}_{n-2}^* = 0 \end{cases}. \tag{13}$$

The considered SV-PWM is quarter-wave symmetric, and it can be analyzed in the range [0, π/2] of the phase angle $\vartheta = \omega t$. The calculation of application times for the first sector (①, k = 1) defined in [19] for 3-phase, in [20] for 5-phase, and in [21] for 7-phase VSIs, can be extended to any sector k by replacing the phase angle ϑ with $\vartheta-(k-1)\pi/n$, k = 1, 2, …, 2n. Note that the modulation limit is defined according to the generalized expression given in [31] for n phases, $m_{max}= [2\ cos\ (\pi/2n)]^{-1}$.

In Fig. 3 are presented the space vector diagrams of the output voltage in the first α-β plane for 3-, 5-, and 7-phase inverters with emphasized the switch configurations and the corresponding voltage vectors involved in the commutation process in the first quadrant. The different colors represent the different sub-cases identified in order to evaluate the current ripple, as explained with details in [19], [20], and [21], respectively.

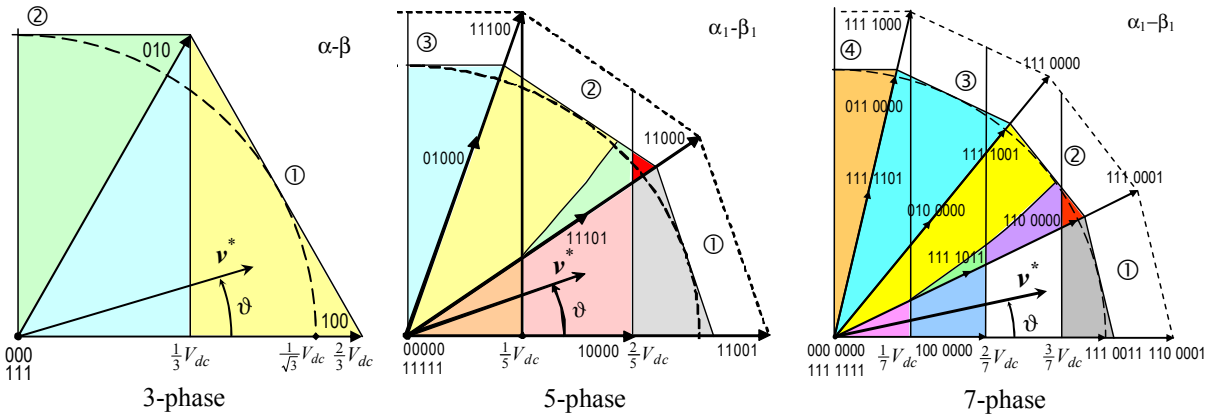

Fig. 3: Space vector diagrams of inverter output voltage in the range ϑ = [0, 90°]. Different colored areas correspond to different equations for determining the current ripple.

Ripple evaluation

Due to the symmetry among all phases in the considered case of sinusoidal balanced currents, only the 1st phase is examined in the analysis. In terms of multiple space vectors, the phase variables are given by (12). For the 1st phase, it results in the sum of the projections of the $(n-1)/2$ space vectors on the real axes. In particular, introducing (13) in (12), the average output voltage of the 1st phase is given by

$$\bar{v}(T_s) = v^* = \sum_{h=1}^{n-2} \Re e\{\boldsymbol{v}_h^*\} = m V_{dc} \cos\vartheta \ , \quad h \quad odd \ . \tag{14}$$

By introducing (14) in (4), and calculating $v(t)$ by (12), the alternating component of inverter output voltage (first phase) can be written as

$$\tilde{v}(t) = \left[S_1 - \frac{1}{n}\left(S_1 + S_2 + \ldots + S_n\right) \right] V_{dc} - m V_{dc} \cos\vartheta, \tag{15}$$

where S_k represents the switch state of the k-th inverter leg, $S_k = [0, 1]$.

In order to evaluate the current ripple in the whole phase angle range $0 < \vartheta < \pi/2$, the different cases corresponding to the different sectors ①, ②, …, depicted in Fig. 3 should be considered, for 3-, 5- and 7-phase inverters, respectively. Ripple is evaluated on the basis of (8), (9), and (15). Additional sub-cases, also determined by the value of modulation index, are identified in Fig. 3 with different colored areas. Peak-to-peak current ripple has been determined accordingly, for 3-phase inverters [19], extended to the case of multiphase inverters, with emphasis on 5-phase inverters [20], and similarly to 7-phase inverters [21].

Comparison of the peak-to-peak current ripple

Peak-to-peak ripple diagrams

In order to show the behavior of the peak-to-peak current ripple amplitude in the fundamental period for the considered cases, in Figs. 4 and 5 is represented the normalized function of the current peak-to-peak ripple amplitude, $r(m,\vartheta)$, defined as

$$\tilde{i}_{pp} = \frac{V_{dc} T_s}{2L} r(m,\vartheta) \ . \tag{16}$$

Fig. 4 shows $r(\vartheta)$ for m = 1/6, 1/3, and 1/2 (from left to right), for 3-, 5-, and 7-phase inverters (blue, red, and green lines, respectively). It can be noted that for low modulation indexes, inverters has similar ripple amplitude, while the more difference rise with higher modulation indexes. In general, the ripple for the 3-phase inverter is lower, whereas 5- and 7-phase inverters have more similar ripple behavior, even for the higher modulation indexes.

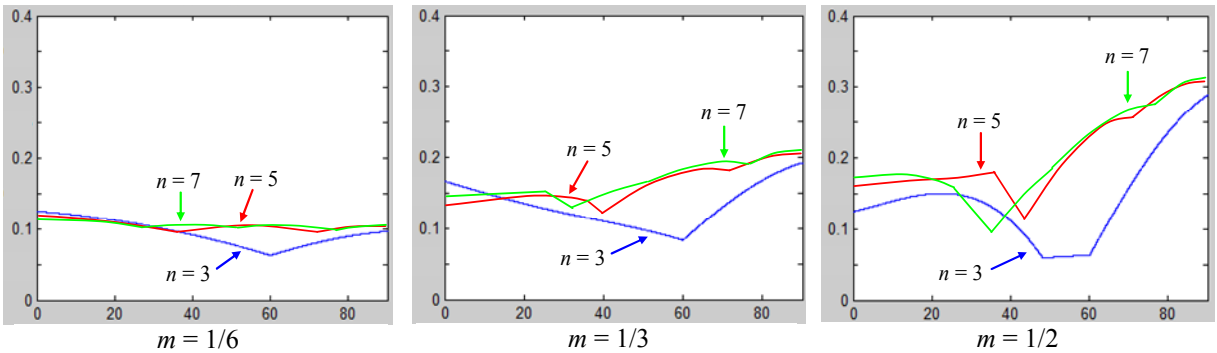

Fig. 4: Normalized peak-to-peak current ripple amplitude $r(m,\vartheta)$ for 3-, 5-, and 7-phase VSIs in the range $\vartheta = [0, 90°]$ for different modulation indexes.

 ISBN: 978-90-75815-17-7 and 978-1-4799-0114-2

Fig. 5 shows the colored map of $r(m,\vartheta)$ for the first quadrant of the α-β plane within the modulation limits for 3-, 5-, and 7-phase inverters, respectively. It can be noted that ripple amplitude is obviously zero for $m = 0$, since the null configurations are the only applied, increasing almost proportionally with m in the neighborhoods of $m = 0$. A phase angle with minimum ripple can be indentified in the range $\vartheta \approx 50°\div60°$ for 3-phase inverter, $\vartheta \approx 40°\div45°$ for 5-phase inverter, and $\vartheta \approx 30°\div35°$ for 7-phase inverter. The phase angle with maximum ripple is $\vartheta = 90°$ for all cases, with ripple amplitude almost proportional to the modulation index. This aspect is further developed in the following sub-section.

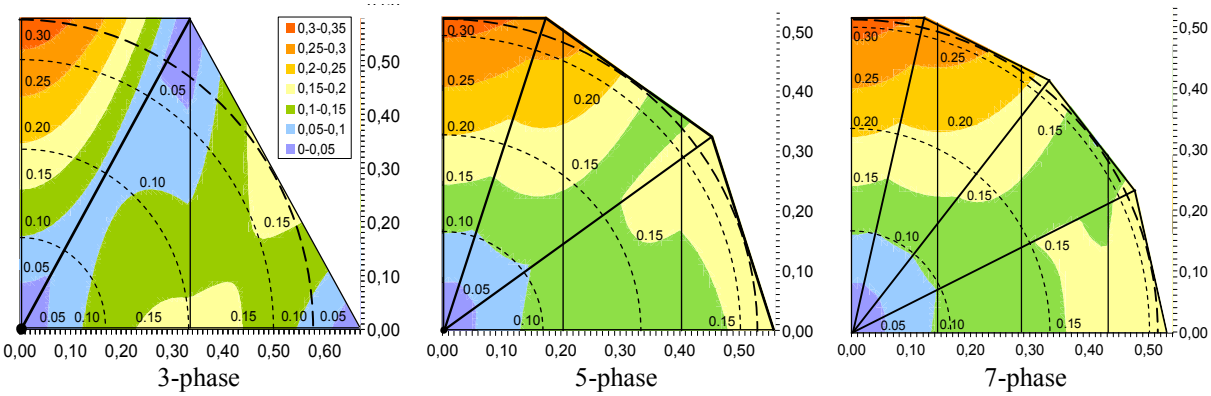

Fig. 5: Map of the normalized peak-to-peak current ripple amplitude $r(m,\vartheta)$ for multiphase VSIs.

Maximum of the peak-to-peak ripple

In order to estimate the current ripple amplitude in the whole fundamental period, the maximum of the current ripple can be evaluated in the phase angle range [0, 90°] as in [19] for 3-phase inverters, in [20] for 5-phase inverters, and in [21] for 7-phase inverters. The composition of the two local maxima of the normalized current ripple is given in Fig. 6, leading to the global maximum r^{max}, for 3-, 5-, and 7-phase inverters. The three vertical dashed gray lines represent the specific modulation indexes, m = 1/6, 1/3, and 1/2, which are further examined in simulations. It can be noted that maximum ripple is almost proportional to the modulation index, just the numeric coefficient is slightly different for different phase number. Then, a simplified expression for maximum of peak-to-peak current ripple amplitude is obtained for the 3-, 5-, and 7-phase inverters

$$\text{3-phase VSI:}\quad \tilde{i}_{pp}^{\,max} \cong \frac{V_{dc}T_s}{3.46L}m\,, \qquad r^{max} \cong 0.578\,m \tag{17}$$

$$\text{5-phase VSI:}\quad \tilde{i}_{pp}^{\,max} \cong \frac{V_{dc}T_s}{3.25\,L}m\,, \qquad r^{max} \cong 0.615\,m \tag{18}$$

$$\text{7-phase VSI:}\quad \tilde{i}_{pp}^{\,max} \cong \frac{V_{dc}T_s}{3.2\,L}m\,, \qquad r^{max} \cong 0.625\,m\,. \tag{19}$$

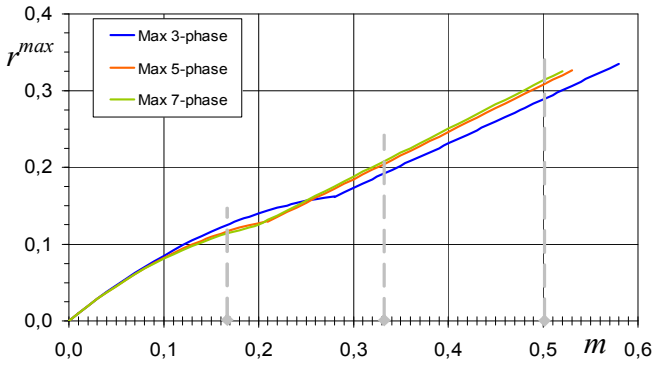

Fig. 6: Maximum of the normalized peak-to-peak current ripple amplitude vs. modulation index.

Numerical results

In order to verify and compare the theoretical developments shown in [19] for 3-phase inverters, in [20] for 5-phase inverters, and in [21] for 7-phase inverters, circuit simulations are carried out by Sim-PowerSystems of Matlab considering a balanced RL load, having $R = 20\ \Omega$ and $L = 3$ mH.

In all simulations the fundamental frequency f is set to 50 Hz, the switching frequency $1/T_s$ is 5.25 kHz, and the dc voltage supply V_{dc} is 600V. A centered symmetrical carrier-based PWM technique is considered, equivalent to the multiple space vector PWM.

The instantaneous current ripple $\tilde{i}$ in simulations is calculated as the difference between the instantaneous current $i(t)$ and its fundamental component $I_{fund}(t)$, for the first phase, i.e.

$$\tilde{i}(t) = i(t) - I_{fund}(t)\,. \tag{20}$$

In all simulations the systems are well balanced and the first phase is selected for further analysis, as in analytical considerations. Different values of m are investigated (1/6, 1/3, and 1/2).

In Figs. 7 (a), 8 (a), and 9 (a) (left columns) the current ripple $\tilde{i}$ calculated by (20) (pink trace), is compared with the half of peak-to-peak current ripple obtained by the analytical developments, $\tilde{i}_{pp}/2$ (blue trace), for 3-, 5-, and 7-phase inverters in one fundamental period, for different values of modulation indexes (1/6, 1/3, and 1/2, respectively). In the corresponding Figs. 7 (b), 8 (b), and 9 (b) (right columns) are depicted the instantaneous output currents with the calculated upper/lower ripple envelope, depicted in blue colors, for the same cases (1/6, 1/3, and 1/2, respectively).

The considered modulation indexes cover most of the possible sub-cases, i.e., most of the colored regions in Fig. 3. The agreement is good in the whole fundamental period, for all cases.

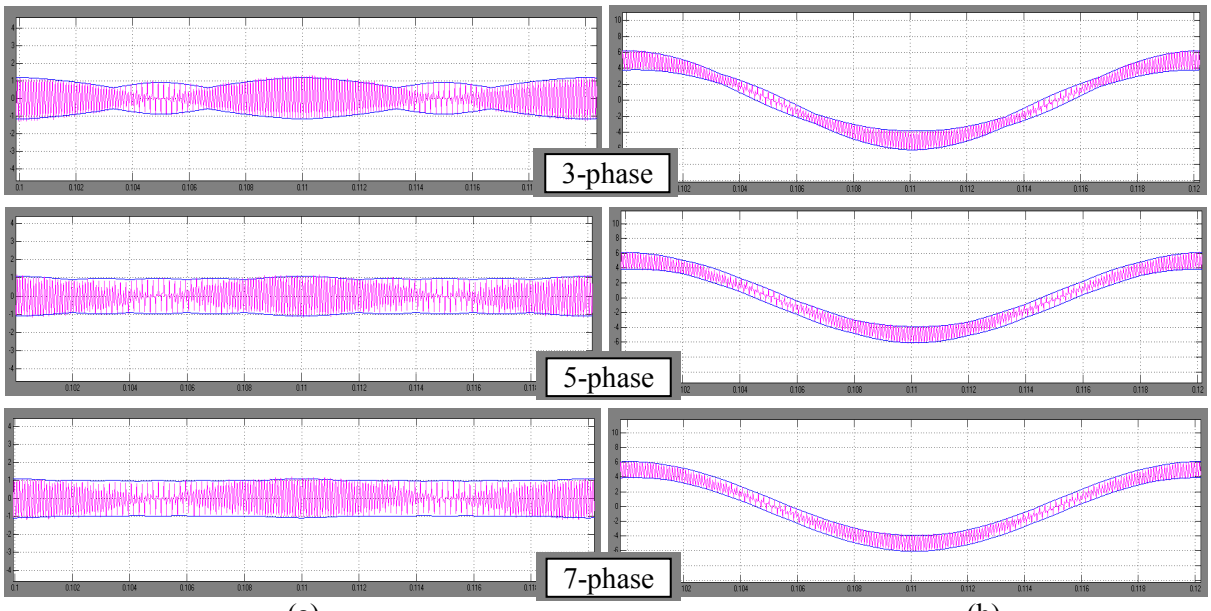

(a) (b)

Fig. 7: Simulation results and calculated current ripple envelopes in a fundamental period for $m = 1/6$ (a) simulated current ripple (pink) with evaluated peak-to-peak amplitude (blue); (b) simulated instantaneous current (pink) with calculated ripple envelopes (blue).

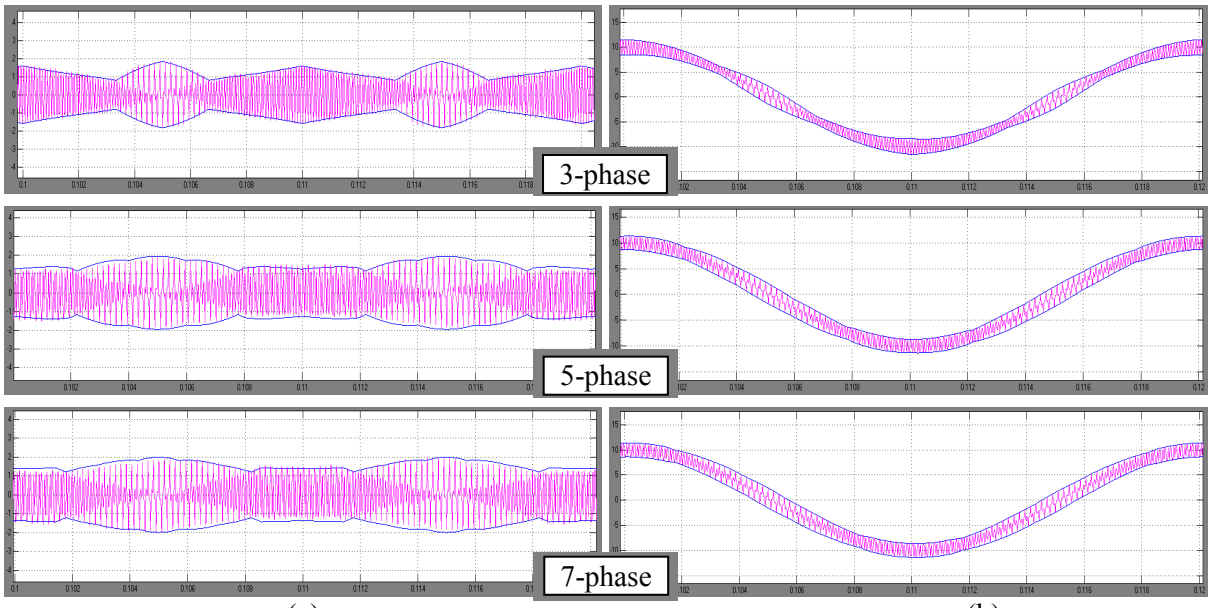

(a) (b)

Fig. 8: Simulation results and calculated current ripple envelopes in a fundamental period for m = 1/3: (a) simulated current ripple (pink) with evaluated peak-to-peak amplitude (blue); (b) simulated instantaneous current (pink) with calculated ripple envelopes (blue).

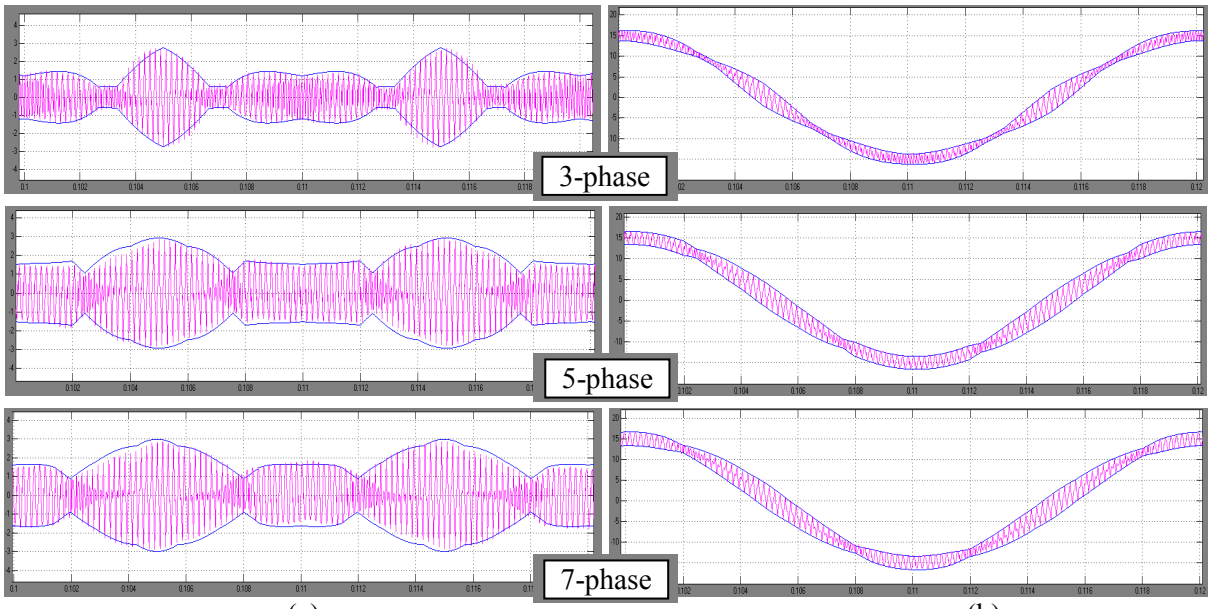

(a) (b)

Fig. 9: Simulation results and calculated current ripple envelopes in a fundamental period for m = 1/2: (a) simulated current ripple (pink) with evaluated peak-to-peak amplitude (blue); (b) simulated instantaneous current (pink) with calculated ripple envelopes (blue).

Conclusion

In this paper the instantaneous output current ripple for multiphase PWM inverters has been identified and compared, starting from 3 phases and extended to case of 5 and 7 phases. In particular, the analytical expressions of peak-to-peak current ripple amplitude, which have been derived for the whole fundamental period as function of the modulation index, are compared among the different phase numbers.

 ISBN: 978-90-75815-17-7 and 978-1-4799-0114-2

Simplified expressions to evaluate the maximum of the current ripple amplitude in the fundamental period, are developed for 3-, 5-, and 7-phase inverters. It has been pointed out that maximum peak-to-peak current ripple amplitude is almost linear function of the modulation index for any phase number, with slightly different coefficient. The peak-to-peak ripple evaluation has been verified by numerical simulations for different values of modulation index by realistic inverter-load circuit models.

Despite of the proposed method is applied to centered symmetrical PWM, the analysis can be readily extended to either discontinuous or asymmetrical modulation, both carrier-based and space vector PWM. Furthermore, the derived analytical expressions can be utilized to minimize the current ripple amplitude by properly adjusting the switching frequency and/or by modifying the sharing of the application time of the zero voltage vector between the two null switch configurations. This could be the topic of further investigations.

References

[1] H.A. Toliyat, S.P. Waikar, T.A. Lipo, "Analysis and simulation of five-phase synchronous reluctance machines including third harmonic of airgap MMF," *IEEE Trans. on Industry Applications*, vol.34, no. 2, pp. 332–339, March/April 1998.

[2] H. Xu, H.A. Toliyat, L.J. Petersen, "Five-phase induction motor drives with DSP-based control system," *IEEE Trans. on Power Electronics*, vol. 17, No. 4, pp. 524–533, July 2002.

[3] H.M. Ryu, J.K. Kim, S.K. Sul, "Synchronous frame current control of multi-phase synchronous motor. Part I. Modelling and current control based on multiple d-q spaces concept under balanced condition," *Proc. of 39th Annual Meeting of IEEE Industry Application Society*, Seattle, Washington, vol. 1, pp. 56–63, 3-7 October 2004.

[4] L. Parsa, H.A. Toliyat, "Five-phase permanent-magnet motor drives," *IEEE Trans. on Industry Applications*, vol. 41, no. 1, pp. 30–37, Jan./Febr. 2005.

[5] G. Grandi, G. Serra, A. Tani, "General analysis of multi-phase systems based on space vector approach," *Proc. of 12th Power Electronics and Motion Control Conference* (*EPE-PEMC*), Portoroz (Slovenia), pp. 834-840, 30 Aug–1 Sept, 2006.

[6] H.M. Ryu, J.W. Kim, S.K. Sul, "Analysis of multi-phase space vector pulse width modulation based on multiple d-q spaces concept," *IEEE Trans. on Power Electronics*, vol. 20, no. 6, pp. 1364–1371, Nov. 2005.

[7] A. Iqbal, E. Levi, "Space vector modulation schemes for a five- phase voltage source inverter," *Proc. of 11th European Conference on Power Electronics and Applications* (*EPE*), Dresden (D), pp. 1–12, Sept. 11-14, 2005.

[8] P.S.N. de Silva, J.E. Fletcher, B.W. Williams, "Development of space vector modulation strategies for five phase voltage source inverters," *Proc. of Power Electronics, Machines and Drives Conference* (*PEMD*), vol. 2, pp. 650–655, 31 Mar–2 Apr, 2004.

[9] O. Ojo, G. Dong, "Generalized discontinuous carrier-based PWM modulation scheme for multi-phase converter-machine systems," *Proc. of 40th Annual Meeting of IEEE Industry Applications Society*, Hong Kong, pp. 1374–1381, 2-6 Oct, 2005.

[10] G. Grandi, G. Serra, A. Tani "Space vector modulation of a seven-phase voltage source inverter," *Proc. of Int. Symposium on Power Electronics*, *Electrical Drives*, *Automation and Motion* (*SPEEDAM*), Taormina, Italy, pp. 1149–1156, 23-26 May 2006.

[11] D. Dujic, E. Levi, G. Serra, A. Tani, L. Zarri "General modulation strategy for seven-phase inverters with independent control of multiple voltage space vectors," *IEEE Transaction on Industrial Electronics,* vol. 55, no. 5, pp. 1921–1932, May 2008.

[12] D. Dujic, E. Levi, M. Jones, G. Grandi, G. Serra, A. Tani, "Continuous PWM techniques for sinusoidal voltage generation with seven-phase voltage source inverters," *Proc. of Power Electronics Specialists Conference* (*IEEE-PESC*), pp. 47–52, 17-21 June 2007.

[13] D. Casadei, M. Mengoni, G. Serra, A. Tani, L. Zarri "A new carrier-based PWM strategy with minimum output current ripple for five-phase inverters," *Proc. of the 14th European Conference on Power Electronics and Applications* (*EPE*), pp. 1–10, 30 Aug –1 Sept, 2011.

[14] D. Dujic, M. Jones, E. Levi, "Analysis of output current ripple rms in multiphase drives using space vector approach," *IEEE Trans. on Power Electronics*, vol. 24, no. 8, pp. 1926–1938, August 2009.

[15] M. Jones, D. Dujic, E. Levi, J. Prieto, F. Barrero "Switching ripple characteristics of space vector PWM schemes for five-phase two-level voltage source inverters-Part2: Current ripple," *IEEE Trans. on Industrial Electronics*, vol. 58, no. 7, pp. 2799–2808, July 2011.

[16] P. A. Dahono, Deni, E. G. Supriatna, "Output current-ripple analysis of five-phase PWM inverters," *IEEE Trans. on Industry Applications*, vol. 45, no. 6, pp. 2022–2029, November/December 2009.

[17] D. Dujic, M. Jones, E. Levi, "Analysis of output current-ripple RMS in multiphase drives using polygon approach," *IEEE Trans. on Power Electronics*, vol. 25, no. 7, pp. 1838–1849, July 2010.

[18] D. Jiang, F. (Fred) Wang "Study of analytical current ripple of three-phase PWM converter," *Proc. of 27th IEEE Applied Power Electronics Conference and Exposition* (*APEC*), pp. 1568– 1575, 5-9 Feb, 2012.

[19] G. Grandi and J. Loncarski, "Evaluation of current ripple amplitude in three-phase PWM voltage source inverters," *Proc. of 8th IEEE Conference-Workshop on Compatibility and Power Electronics* (*CPE*), Ljubljana (SLO), 5-7 June 2013.

[20] G. Grandi and J. Loncarski, "Evaluation of current ripple amplitude in five-phase PWM voltage source inverters," *Proc. of IEEE Conference on ICT, Power engineering, and Signal processing* (*EUROCON*), Zagreb (CRO), 1-4 July 2013.

[21] G. Grandi and J. Loncarski, "Analysis of Peak-to-Peak Current Ripple Amplitude in Seven-Phase PWM Voltage Source Inverters", under review, *Energies*, 6, ISSN 1996-1073, 2013.

[22] G. Grandi, J. Loncarski, R. Seebacher, "Effects of current ripple on dead-time distortion in three-phase voltage source inverters," *in Proc. of 2nd IEEE ENERGYCON Conference & Exhibition - Advances in Energy Conversion*, Florence, Italy, pp. 207-212, 9–12 Sept, 2012.

[23] M.A. Herran, J.R. Fischer, S.A. Gonzalez, M.G. Judewicz, , D.O. Carrica, "Adaptive dead-time compensation for grid-connected PWM inverters of single-stage PV systems," *IEEE Trans. on Power Electronics*, vol.28, no.6, pp. 2816–2825, June 2013.

[24] J.M. Schellekens, R.A.M. Bierbooms, and J.L. Duarte, "Dead-time compensation for PWM amplifiers using simple feed-forward techniques," *in Proc. of XIX Int. Conference on Electrical Machines* (*ICEM*), pp. 1–6 Sept, 2010.

[25] X. Mao, R. Ayyanar, H. K. Krishnamurthy, "Optimal variable switching frequency scheme for reducing switching loss in single-phase inverters based on time-domain ripple analysis," *IEEE Trans. on Power Electronics*, vol.24, no.4, pp. 991–1001, April 2009.

[26] C. Ngai-Man Ho, V.S.P. Cheung, and H. Shu-Hung Chung, "Constant-frequency hysteresis current control of grid-connected VSI without bandwidth control," *IEEE Trans. on Power Electronics*, vol. 24, no. 11, pp. 2484 – 2495, Nov. 2009.

[27] D.G. Holmes, R. Davoodnezhad, and B.P. McGrath, "An improved three-phase variable-band hysteresis current regulator," *IEEE Trans. on Power Electronics*, vol. 28, no. 1, pp. 441–450, Jan. 2013.

[28] D. Jiang and F. Wang, "Variable switching frequency PWM for three-phase converter for loss an d EMI improvement," *In Proc. of 27th IEEE Applied Power Electronics Conference and Exposition* (*APEC*), Orlando, Florida, pp. 1576-1583, 2012.

[29] D. Casadei, G. Serra, A. Tani, L. Zarri "Theoretical and experimental analysis for the RMS current ripple minimization in induction motor drives controlled by SVM technique," *IEEE Trans. on Industrial Electronics*, vol. 51, no. 5, pp. 1056-1065, Oct. 2004.

[30] A. Iqbal and S. Moinuddin, "Comprehensive relationship between carrier-based PWM and space vector PWM in a five-phase VSI,", *IEEE Trans. on Power Electronics*, vol.24, no.10, pp. 2379–2390, Oct. 2009.

[31] E. Levi, D. Dujic, M. Jones, G. Grandi, "Analytical determination of DC-bus utilization limits in multiphase VSI supplied AC drives," *IEEE Trans. on Energy Conversion*, vol. 23, no. 2, pp. 433–443, June 2008.